J Mater Sci (2011) 46:7106–7113
DOI 10.1007/s10853-011-5407-x

SIZE DEPENDENT EFFECTS

Soft mechanochemically assisted synthesis of nano-sized $LiCoO_2$ with a layered structure

E. Grigorova · T. S. Mandzhukova · M. Khristov · M. Yoncheva · R. Stoyanova · E. Zhecheva

Received: 8 January 2011 / Accepted: 17 February 2011 / Published online: 2 March 2011

Abstract Soft mechanochemically assisted reaction between CoOOH and $LiOH{\cdot}H_2O$ at 400 °C yields *O3*-layered $LiCoO_2$ with nanometric particle sizes of 20–30 nm. The interaction of CoOOH with $LiOH{\cdot}H_2O$ is monitored by DTA and TGA analysis. XRD powder and TEM analysis is used for structural and morphological characterization of the precursors and target $LiCoO_2$. Soft mechanochemical treatment of the CoOOH–$LiOH{\cdot}H_2O$ mixture leads to amorphization of the lithium salt, while CoOOH remains intact. In addition, a partial exchange of protons from CoOOH with lithium takes place. Thermal treatment at 400 °C of the mechanochemically treated mixture yields layered $LiCoO_2$ with a small amount of a spinel-type $Li_{2+y}Co_{2-y}O_4$ phase (less than 2%). The morphology of $LiCoO_2$ inherits the morphology of CoOOH in the precursor. Layered $LiCoO_2$ displays thin nanometric particles with a narrow particle size distribution: more than 50% of particles are distributed between 20 and 30 nm. The electrochemical extraction and insertion of lithium in nano-sized $LiCoO_2$ is examined in model lithium cells using a galvanostatic mode.

Introduction

In the last 15 years, lithium cobaltate, $LiCoO_2$, has been considered as a material of great scientific importance due to its application as a cathode material in high-power lithium ion batteries [1]. The research interest has recently been renewed due to the discovery of thermoelectric properties of layered sodium cobaltates [2]. The application of lithium cobaltate is based on its ionic, electronic and thermal conductivity properties, which are, to a great extent, size-dependent [3, 4].

To get a good performance of $LiCoO_2$, there is a need to elaborate a synthesis method which is capable to produce $LiCoO_2$ with uniform nano-particles. In this aspect, various chemical processes have been reported: freeze-drying [5, 6], ultrasonic process, and modified Pechini process [7], sonochemical synthesis [8], precipitation and aging process [9], hydrothermal synthesis [10, 11] and organometallic precursors [5, 12]. However, the fabrication of nano-sized $LiCoO_2$ is a difficult task, because $LiCoO_2$ has four structural varieties. The stable structural modification of $LiCoO_2$ is the layered one, which is usually obtained at high temperatures (higher than 600 °C) [13, 14]. The crystal structure (space group *R*-3 m) is composed of consecutively arranged Li^+ and Co^{3+} ions in the close-packed oxygen arrays, as a result of which discrete lithium and cobalt layers are formed [14]. Between the layers, LiO_6 and CoO_6 octahedra share common edges so that three CoO_2-layers are needed to describe the unit cell of $LiCoO_2$ (*O3*-form, according to the notation of Delmas et al. [15]). At a low temperature (about 400 °C), a new modification of $LiCoO_2$ with a spinel-related structure has been prepared by a solid state reaction between lithium carbonate and cobalt oxide [16–18]. The spinel modification is also denoted as the low-temperature (LT) modification in opposition to the rhombohedral high-temperature modification (HT). In an analogy with *O3*–$LiCoO_2$, the structure of LT-$LiCoO_2$ can be derived from the close oxygen packing, whereas Li and Co ions occupy the two octahedral sites in a 3:1 (or 1:3) ratio, thus leading to a spinel modification (structural type $Li_2Ti_2O_4$). Above 600 °C, the spinel-related phase is transformed into the layered *O3*-modification. The mechanochemical synthesis is considered

E. Grigorova · T. S. Mandzhukova · M. Khristov · M. Yoncheva · R. Stoyanova · E. Zhecheva (✉)
Institute of General and Inorganic Chemistry, Bulgarian Academy of Sciences, 1113 Sofia, Bulgaria
e-mail: zhecheva@svr.igic.bas.bg

as an appropriate method for the preparation of $LiCoO_2$ with a spinel-related structure [19–21]. The advantage of this method is the reduction of the reaction temperature and the reaction time for the formation of $LiCoO_2$. Recently, two metastable polytypes of $LiCoO_2$ have been prepared by ion-exchange reactions [22–26]. Their structures are composed of the same LiO_2 and CoO_2-layers, but the type of the layer stacking along the c_{hex} axis is different. Among the structural varieties of $LiCoO_2$, the *O3*-layered modification with nano-metric particles is of research interest as a cathode and thermoelectric material [1, 27, 28].

In this contribution, we report new data on the formation of nano-sized $LiCoO_2$ with a layered crystal structure by applying a mechanochemically assisted reaction of CoO-OH with $LiOH.H_2O$. Since the morphology of the pristine compound has been shown to affect the morphology of the target compound, we have used nano-sized CoOOH for the synthesis of nano-sized $LiCoO_2$. The crystal structure of CoOOH is built from CoO_2-layers, which are the common structural element of CoOOH and $LiCoO_2$. Another advantage for the use of CoOOH is its ability to exchange proton with lithium, thus forming $Li_{1-x-y}H_yCoO_2$ compositions with $x \leq 0.55$ and $x + y < 1$ [29, 30]. Lithium hydroxide is characterized with a good plasticity, which determines a good adhesion of LiOH toward the oxides during the mechanochemical treatment [31]. In order to stabilize the layered modification of $LiCoO_2$, the Li-to-Co ratio in the precursors was changed from 1 to 1.5. The interaction of CoOOH with $LiOH{\cdot}H_2O$ was monitored by DTA and TGA analysis. XRD powder and TEM analysis was used for structural and morphological characterization of precursors and target $LiCoO_2$. The formation of nano-sized $LiCoO_2$ with a layered crystal structure is demonstrated by electrochemical extraction and insertion of lithium.

Experimental

The starting reagents were $Co(NO_3)_2{\cdot}6H_2O$ (Aldrich, ACS reagent, ≥98%) and $LiOH{\cdot}H_2O$ (Aldrich, 99.95% trace metals basis). Mechanochemically assisted reaction between CoOOH and $LiOH.H_2O$ followed by heating at 400 °C was applied for the preparation of $LiCoO_2$. The mechanochemical synthesis proceeded in a planetary monomill Fritsch Pulverisette 6 using agate balls (diameter = 10 mm) and agate container (volume ≈ 75 cm^3). The experimental conditions were as follows: the milling was in an air atmosphere, the weight ratio of powder samples to balls was 1:13, the rotation speed was 200 rpm and the ball milling duration was for 10 h. CoOOH was obtained by oxidation of freshly precipitated β-$Co(OH)_2$ with oxygen at room temperature, according to the method described by Delaplane et al. [32]. This method allows preparing thin particles of CoOOH as was shown in [30]. The Li-to-Co ratio is 1.00, 1.22, and 1.50. The excess of lithium is used in order to avoid the possible lithium losses during mechanochemical treatment.

The lithium and cobalt content in the samples were determined by ICP analysis. The mean oxidation state of cobalt was determined by iodometric titration against a standardized sodium thiosulfate solution. Iodometric titration was performed on 10-20 mg of sample in Ar atmosphere. For each composition the titrations were repeated several times in order to obtain accurate and consistent results.

X-ray phase analysis was performed using a Bruker Advance D8 diffractometer with detector Sol-X and and CuKα radiation. The scan range was $15 \leq 2\theta \leq 120$ ° with a step increment of 0.02°. A Fullprof computer programme was used for the calculations [33]. The diffractometer point zero, the Lorentzian/Gaussian fraction of the pseudo-Voigt peak function, scale factor, the unit cell parameters, the oxygen parameter, the thermal factor for the trigonal and spinel positions, the line half-width parameters and the preferred orientation were determined.

The thermal analysis (simultaneously obtained DTA-, TG-, DTG-, and evolved gas curves) of the precipitated compositions was carried out by a combined LABSYS^{TM} EVO DTA/TG system of the SETARAM Company, France, with a gas-analyser of the OmniStar^{TM} type. The samples are investigated at a heating rate of 10 °C/min in O_2 flow (20 ml/min).

The TEM investigations were performed by TEM JEOL 2100 at accelerating voltage of 200 kV. The specimens are prepared by grinding and dispersing them in ethanol by ultrasonic treatment for 6 min. The suspensions are dripped on standard holey carbon/Cu grids.

The electrochemical charge–discharge of $LiCoO_2$ was carried out by using two-electrode cells of the type Li | $LiPF_6$ (EC:DMC) | $LiCoO_2$. The positive electrode, supported onto an aluminum foil, was a mixture containing 80% of the active composition $LiCoO_2$, 7.5% C-NERGY KS 6 L graphite (TIMCAL), 7.5% Super C65 (TIMCAL) and 5% polyvinylidene fluoride (PVDF). The electrolyte was 1 M $LiPF_6$ solution in ethylene carbonate and dimethyl carbonate (1:1 by volume) with less than 20 ppm of water. Lithium electrodes consisted of a clean lithium metal disk with diameter in 15 mm. The electrochemical reactions were carried out using an eight-channel Arbin BT2000 system in galvanostatic mode. The cells are mounted in a dry box under Ar atmosphere. The cell was cycled between 4.3 and 2.2 V at C/20 rate.

Results

Structure of mechanochemical treated CoOOH–LiOH·H_2O precursors

Effective mechanochemical treatment of a mixture of CoOOH and LiOH has been shown to produce amorphization of both CoOOH and LiOH components [31]. In addition, a spinel-related phase with a lower degree of crystallinity was also established [31]. To avoid the degradation of the layered structure of CoOOH, we have used a soft mechanochemical treatment. Figure 1 gives the XRD patterns of mechanochemically treated CoOOH–LiOH·H_2O mixture with Li/Co = 1.5. The XRD patterns consist of well-resolved diffraction peaks due to CoOOH (rhombohedral modification, *R-3m* space group) together with low-intensity peaks due to a cobalt spinel phase. The amount of the spinel phase is about 2% and does not depend on the Li-to-Co ratio in the precursor (Table 1). It is noticeable that neither lithium hydroxide nor other lithium salts (such as Li_2CO_3) are observed, even for the precursor with the highest Li-to-Co ratio. This means that the mechanochemical treatment used leads to amorphization of the lithium salt, but CoOOH retains its crystallinity.

The lattice parameters of CoOOH and the spinel phase are shown in Table 1. Untreated CoOOH has an interplanar distance of 4.38 Å, which coincides with the structural data of Delaplane et al. [31]. After mechanochemical treatment, the *c*-lattice parameter of CoOOH undergoes slight changes with increasing the Li-to-Co ratio in the precursor, while the *a*-parameter remains intact (Table 1). It appears that the mechanochemical treatment leads to an extension of the interplanar distance with preservation of the intralayer distance between the metal ions. This trend suggests for some exchange of protons with lithium ions during the mechanochemical treatment. It is worth to mention that a partial exchange of protons and lithium with the formation of a $Li_{1-x-y}H_yCoO_2$ composition with $x \leq 0.55$ and $x + y < 1$ has also been established during the decomposition of CoOOH in a $LiNO_3$ melt, as well as during acid digestion of $LiCoO_2$ with concentrated acid [29, 30]. Based on first principle calculations of the free energy of the proton-for-lithium ion exchange reactions, it has been found that the protonation is energetically most favorable for layered $LiCoO_2$ [34]. Concerning the spinel phase, the lattice parameter does not coincide with that of pure Co_3O_4 reported in [35]. This indicates that small amount of Li^+ is incorporated into the spinel structure.

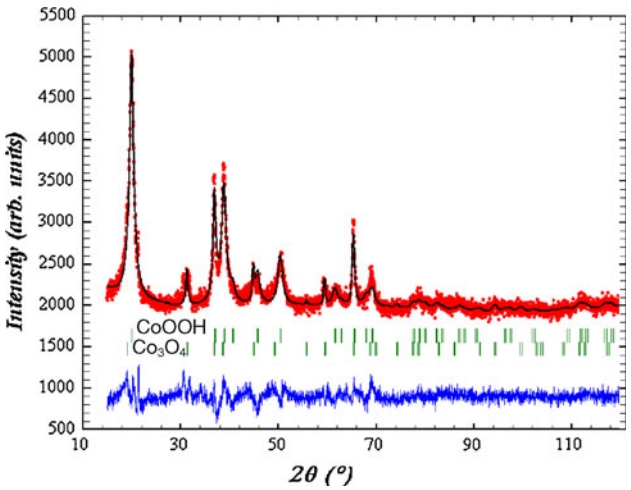

Fig. 1 XRD patterns of mechanochemically treated "CoOOH–LiOH.H_2O" mixture with Li/Co = 1.5. The Brag positions for CoOOH and cobalt spinel are indicated

An important feature of the use of CoOOH as a starting reagent is its morphology. Figure 2 shows the TEM image of the mechanochemically treated CoOOH- LiOH.H_2O mixture with Li/Co = 1.5. The mixture consists of thin nanometric particles with a narrow particle size distribution: more than 80% of the particles are distributed between 20 and 40 nm (Fig. 2). The polycrystalline electron diffraction reveals that the precursor contains CoOOH, cobalt spinel, cobalt oxide and lithium carbonate (Fig. 2). By XRD experiments, CoOOH and cobalt spinel are only detected. This supports the suggestion that lithium hydroxide becomes amorphous during treatment, while the crystallinity of CoOOH is preserved.

Thermal analysis permits to follow the formation of lithium cobaltate from the mechanochemically treated precursors. Figure 3 gives the DTA and TGA curves and the curves of the evolved H_2O and CO_2 gases of the mechanically treated CoOOH–LiOH·H_2O mixture with Li/Co = 1.5. For the sake of comparison, the thermal curves of pristine CoOOH are also given. Pristine CoOOH displays two endothermic effects between 220 and 390 °C accompanied with a weight loss of 11.6% due to H_2O release. Based on the thermal studies of CoOOH [30, 36], this process is related with the decomposition of CoOOH to Co_3O_4 with a total weight loss of 12.7%. The DTA and TG curves of the mechanochemically treated CoOOH–LiOH·H_2O mixture display three broader endothermic peaks. Up to 150 °C, there is a H_2O release accompanied with a weight loss of about 3.9%. This process corresponds to the dehydratation of LiOH·H_2O from the mechanochemically treated LiOH·H_2O–CoOOH mixture. However, the theoretical weight loss of the dehydratation process for this mixture is 17.4%. As one can see, the experimentally determined weight loss is lower than the calculated one. This discrepancy reveals that the lithium hydroxide is partially dehydrated during the mechanochemical treatment. In addition, a partial carbonization of LiOH can not be rejected.

Table 1 Unit cell parameters of CoOOH and $Li_xCo_{3-x}O_4$ in the precursor mixture "CoOOH–LiOH", as well as of layered (*R-3m*) and spinel (*Fd3m*) phases of $LiCoO_2$ in the target product

Li-to-Co ratio (in the precursor)	Li-to-Co ratio (in target product)	CoOOH (precursor)		$Li_xCo_{3-x}O_4$ (precursor)	RA, %	$LiCoO_2$ (*R-3m*)		$LiCoO_2$ (*Fd3m*)		RA (%)
		$a \pm 0.0003$ (Å)	$c \pm 0.0040$ (Å)	$a \pm 0.001$ (Å)		$a \pm 0.0003$ (Å)	$c \pm 0.0040$ (Å)	$a \pm 0.0014$ (Å)	$x_{Li} \pm 0.05$	
Li/Co = 1.0	0.99	2.8519	13.1383	8.080	2.0	2.8135	14.0750	7.9722	0.10	1.3
Li/Co = 1.2	1.19	2.8480	13.2213	8.058	2.5	2.8140	14.0783	7.9725	0.15	2.0
Li/Co = 1.5	1.41	2.8511	13.3048	8.076	2.2	2.8137	14.0783	7.9708	0.15	2.2
HT-$LiCoO_2$						2.8154	14.0507			
LT-$LiCoO_2$ [16]								8.002		
CoOOH [32]		2.851	13.150							
Co3O4 [35]				8.0835						

RA denotes the relative amount of spinel phases in the precursor and the target product. For the sake of comparison, the unit cell parameters of CoOOH, Co_3O_4, HT-$LiCoO_2$ and LT-$LiCoO_2$ are also given

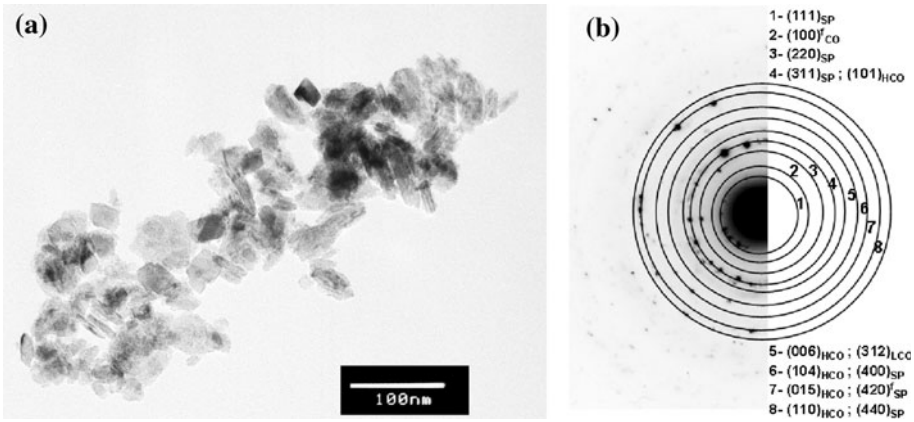

Fig. 2 Bright field micrograph of mechanochemically treated "CoOOH–LiOH.H_2O" mixture with Li/Co = 1.5 (**a**). Polycrystalline electron diffraction (**b**) corresponding to the mixture of CoOOH (HCO, allowed and forbidden reflections), cobalt spinel (SP, allowed and forbidden reflections), cobalt oxide (CO, forbidden reflection) and lithium carbonate (LCO)

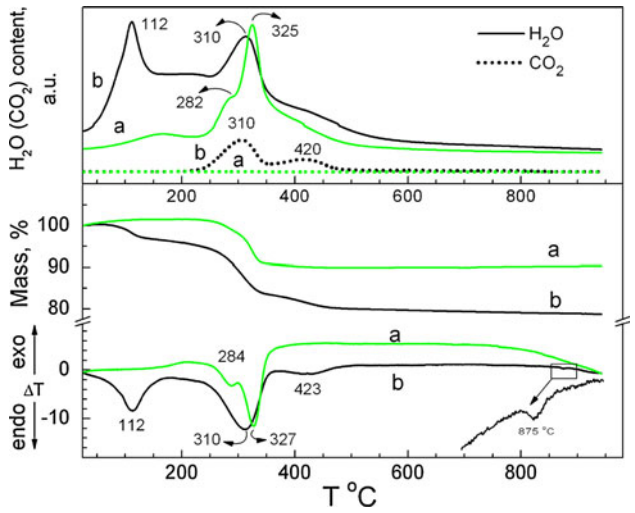

Fig. 3 DTA, TG, and evolved gas analysis curves of pristine CoOOH (**a**) and mechanochemically treated "CoOOH–LiOH·H_2O" mixture with Li/Co = 1.5 (**b**)

In comparison with pristine CoOOH, the decomposition of CoOOH from the mechanochemically treated CoOOH–LiOH·H_2O mixture is a more complex process and proceeds in a broader temperature range (Fig. 3). It appears that the decomposition of CoOOH starts at a slightly lower temperature: 220 °C for pristine CoOOH and 190 °C for the mechanochemically treated CoOOH. This can be related with the partial incorporation of Li^+ into CoOOH. Between 190 and 370 °C, there is a strong endothermic peak with a 13.0% weight loss, followed by a weak endothermic peak with 3.6% weight loss between 370 and 500 °C. In this temperature range, both H_2O and CO_2 gases are evolved. The appearance of carbonate species can be related with partial carbonization of CoOOH during the mechanochemical treatment. (The effect of possible Li_2CO_3 contamination has not to be taken into account, since Li_2CO_3 decomposes at temperatures higher than 700 °C, which is outside the temperature range studied.) It is worth to mention that the endothermic peak at 450 °C due to LiOH melting is not observed.

The close inspection of the DTA curve of the CoOOH–LiOH·H_2O mixture reveals a weak endothermic effect at 876 °C (Fig. 3). This thermal effect can be assigned on the basis of previous studies on the crystal structure and thermal properties of Li-containing Co_3O_4 spinels [30, 37, 38].

It has been found that at a temperature higher than 900 °C, the Co_3O_4 spinel is decomposed into CoO with a rock-salt type structure. The replacement of Co by Li has been shown to suppress the temperature of the spinel-rock salt transition [30, 37, 38]. Therefore, the weak endothermic effect can be attributed to the decomposition of the Li-containing Co_3O_4 spinel to a rock-salt cobalt oxide. This result is consistent with the phase analysis of the CoOOH–$LiOH{\cdot}H_2O$ precursor.

Structure and morphology of nano-sized $LiCoO_2$

At 400 °C and a short heating time (4 h), the thermal decomposition of the mechanochemically treated CoOOH–$LiOH{\cdot}H_2O$ mixture yields layered lithium cobaltate containing impurities of the spinel modification. Figure 4 presents the XRD patterns of $LiCoO_2$ obtained from the precursor with Li/Co = 1.5. Irrespective of the Li-to-Co ratio in the precursor mixture, the XRD patterns are satisfactory fitted by the Rietveld analysis on the basis of two-phase model comprising ideal trigonal and spinel structures (s.g. *R-3m* and s.g. *Fd3m*, Fig. 4). In the trigonal phase, Li and Co ions reside in their usual *3b* and *3a* positions. The crystal structure of the spinel phase includes Li and Co at the *16d* and *16c* spinel positions, as in the case of the $Li_2Ti_2O_4$-type structure. The amount of the spinel phase is less than 2% and does not depend on the Li-to-Co ratio. The origin of the layered and spinel phases can be related with the phase composition of the precursors. It appears that the interaction of CoOOH with the lithium salts leads to the formation of the prevalent layered $LiCoO_2$ phase, while the spinel $LiCoO_2$ phase is a result of the interaction of the Li-containing Co_3O_4 spinel with the lithium salts. The formation of the layered modification of $LiCoO_2$ at low temperature can be related with the good crystallinity of CoOOH, as well as with the good adhesion of the lithium hydroxide to the CoOOH particles. This is a result of the soft mechanical treatment. It is noticeable that the high-energy mechanical treatment produces significant changes in the structure of CoOOH, as a result of which the low-temperature modification of $LiCoO_2$ is formed when the mixture is heated at low temperatures [31].

The structural parameters are given in Table 1. For both layered and spinel phases, the lattice parameters seem to be insensitive toward the Li-to-Co ratio in the precursor mixture. The prevalent phase with a layered structure exhibits lattice parameters that are slightly different from those typical for the high-temperature modification of $LiCoO_2$: the *a*-parameter is slightly lower, while the *c*-parameter is slightly higher (Table 1). The physical meaning of the observed trend is not clear. Contrary to the layered modification, the lattice parameter of the spinel phase is close

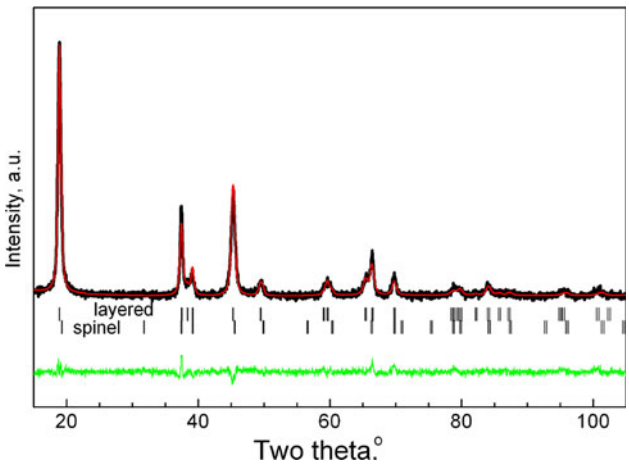

Fig. 4 XRD pattern of $LiCoO_2$ obtained at 400 °C from precursor with Li/Co = 1.5. The Bragg reflections due to layered and spinel modification are shown

to that of the low-temperature modification of $LiCoO_2$ (LT–$LiCoO_2$). The lower amount of the spinel phase does not permit to specify the exact content of Li in the spinel phase. Recently, we have demonstrated that the spinel phase is able to uptake excess lithium, thus forming a $Li_{2+y}Co_{2-y}O_4$ phase without changing the lattice parameter [39].

The evolution of the morphology of lithium cobaltates is demonstrated on Fig. 5. The morphology of CoOOH in the precursor is preserved after heating at 400 °C: thin particles with sizes varying between 20 and 30 nm prevail. The polycrystalline electron diffraction reveals the formation of layered $LiCoO_2$ and lithium carbonate (Fig. 5). The analysis of TEM images shows that nano-sized $LiCoO_2$ is characterized with a narrow particle size distribution (Fig. 6): more than 50% of particles is distributed between 20 and 30 nm.

It is worth to mention that soft mechanochemically assisted reaction yields layered $LiCoO_2$ with particle dimensions, which are among the smallest dimensions as reported in the literature. Layered $LiCoO_2$ obtained by the freeze-drying method [40] and by rapid thermal annealing [28] displays particle sizes varying between 50 and 60 nm. By the mechanochemical method, Choi et al. [41] have reported the preparation nano-crystalline layered $LiCoO_2$ with nano-grain sizes of 70–300 nm. Layered $LiCoO_2$ with mean particle diameter of 20 nm have been prepared by sonochemical synthesis in an aqueous solution of lithium hydroxide containing cobalt hydroxide at 80 °C without any further heat treatment at high temperature [8]. At 600 °C, the interaction between lithium acetate and cobalt acetate in an excess of the lithium salt produces spherical $LiCoO_2$ particles with a diameter of about 25 nm or needle-like $LiCoO_2$ particles with a diameter of about 5 nm and a length of about 60 nm [27].

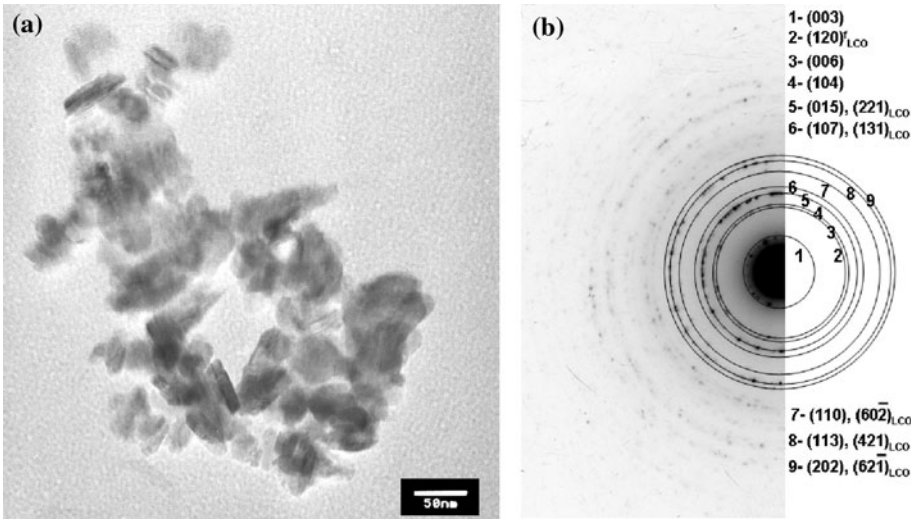

Fig. 5 Bright field micrograph of $LiCoO_2$ obtained at 400 °C from precursors with Li/Co = 1.5 (**a**). Polycrystalline electron diffraction (**b**) corresponding to the mixture of layered $LiCoO_2$ and lithium carbonate (LCO)

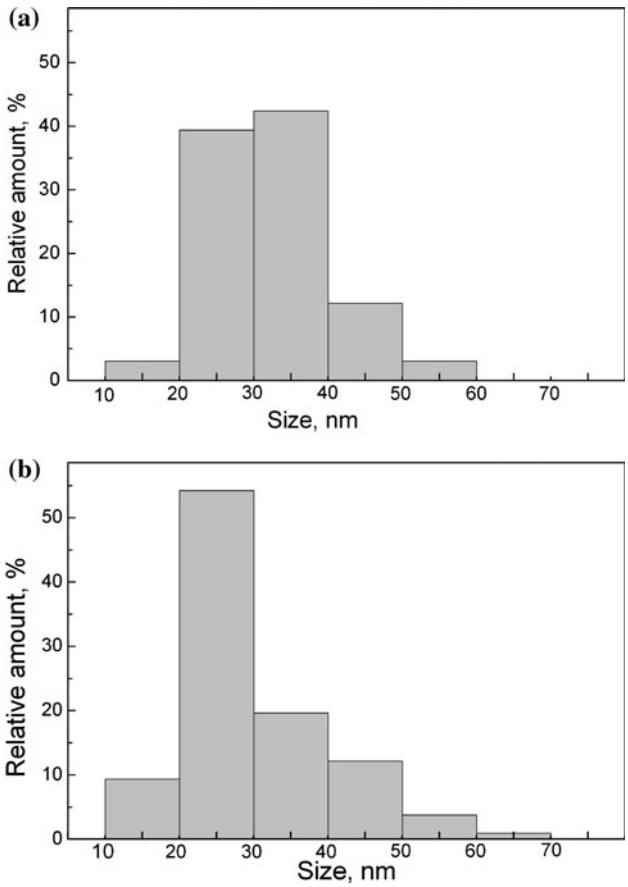

Fig. 6 Particle size distribution of "CoOOH–LiOH·H_2O" mixture (**a**) and $LiCoO_2$ obtained at 400 °C from precursor with Li/Co = 1.5 (**b**)

The ability of nano-sized layered $LiCoO_2$ to intercalate and deintercalate lithium is demonstrated on Fig. 7. The derivatives of the first charge and discharge curves of nano-sized $LiCoO_2$ show the typical electrochemical behavior of the HT-$LiCoO_2$: the main oxidation peak is observed at 3.92 V, and the main reduction peak at 3.87 V. The charge and discharge capacities correspond to 108 and 92 mAh/g, respectively. These effects are related with the Co^{3+}/Co^{4+} redox couple [42]. The electrochemical test supports once again that nano-sized $LiCoO_2$ exhibits the layered structural modification. It is worth mentioning that for nano-sized $LiCoO_2$, the polarization is reduced in comparison with HT-$LiCoO_2$ having particles dimensions of about 2 μm: 0.05 versus 0.07 V (Fig. 7). It is noticeable that the nano-sized $LiCoO_2$ displays sharper peaks, as compared to the peaks of micro-sized HT-$LiCoO_2$. However for nano-sized $LiCoO_2$, the two small peaks between 4.10 and 4.15 V, which are ascribed to an order–disorder transition of the Li^+ ions in the interlayer [43], are not visible. Previous studies on HT-$LiCoO_2$ have shown that the two high-voltage peaks were only observed for highly crystalline samples [44, 45]. The change in the mechanism of the electrochemical reaction in the initial stage of Li extraction is also established for layered $LiCoO_2$ containing over-stoichiometric Li^+ ions (i.e., $Li_{1+t}Co_{1-t}O_{2-t}$ with $t \sim 0.04$) [46]. Therefore, the lack of the order–disorder transition of Li^+ ions in the interlayer space for nano-sized $LiCoO_2$ can be related with some structural disorder. On its turn, this has an effect on the lattice parameters of nano-sized $LiCoO_2$ (Table 1).

Conclusions

Soft mechanochemical treatment of a CoOOH–LiOH·H_2O mixture leads to the amorphization of the lithium salt, the crystallinity of CoOOH being preserved. The amorphization process is accompanied by a partial exchange of proton of CoOOH with lithium, resulting in a lattice expansion along the *c*-axis. In addition, there is a partial transformation of CoOOH into a lithium containing Co_3O_4 spinel (less

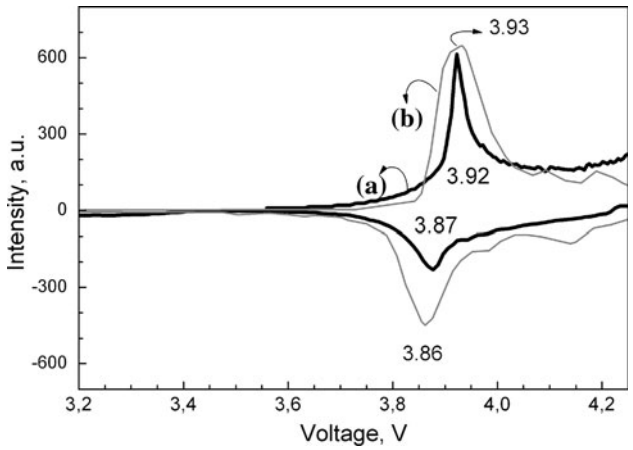

Fig. 7 Derivative of the first charge and discharge curves of $LiCoO_2$ obtained at 400 °C from precursor with Li/Co = 1.5 (*a*). For the sake of comparison, the first charge and discharge curves of HT-$LiCoO_2$ (*grey lines*, *b*) are also given

than 2%). The mechanochemical treated CoOOH–LiOH·H_2O mixture consists of thin nanometric particles with a narrow particle size distribution: more than 80% of particles are between 20 and 40 nm.

The high crystallinity of CoOOH, as well as the good adhesion of lithium hydroxide toward CoOOH, facilitates the formation of the layered modification of $LiCoO_2$ during heating of the CoOOH–LiOH·H_2O mixture at a low temperature (400 °C) and a short heating time (4 h). The layered phase is contaminated by a spinel-related $Li_{2+y}Co_{2-y}O_4$ phase in amount less than 2 wt%. The morphology of layered $LiCoO_2$ inherits the morphology of the CoOOH–LiOH precursor: thin particles with sizes varying between 20 and 30 nm prevail. Nano-sized-layered $LiCoO_2$ is characterized with narrow particle size distribution.

Electrochemical extraction and insertion of lithium in nano-sized $LiCoO_2$ proceed in the potential range which is typical for the HT-modification of $LiCoO_2$. The nano-sized dimensions of the electrode material reduce the cell polarization. Nano-sized $LiCoO_2$ does not display the order–disorder transition of Li^+ ions in the interlayer space. Although the voltage range and the electrolyte composition are not optimized, the results obtained demonstrate, on the one hand, the ability of nano-sized layered $LiCoO_2$ to intercalate lithium reversibly at potential of 4 V. On the other hand, the formation of nano-sized layered $LiCoO_2$ by using a simple method is essential in respect of potential application of $LiCoO_2$ as a cathode material for lithium ion batteries.

Acknowledgements Authors are grateful to the financial support from the National Science Fund of Bulgaria (IDEAS No D0-02-309/2008). Partial financial support by the National Centre for New Materials UNION (Contract No DO-02-82/2008) is also acknowledged. We are grateful of TIMCAL Company for providing carbon additives.

References

1. Ellis BL, Lee KT, Nazar LF (2010) Chem Mater 22:691
2. Terasaki I, Sasago Y, Uchinokura K (1997) Phys Rev B 56:R12685
3. Poizot P, Laruelle S, Grugeon S, Dupont L, Tarascon JM (2000) Nature 407:496
4. Maier J (2005) Nat Mater 4:805
5. Zhecheva E, Stoyanova R, Gorova M, Alcantara R, Morales J, Tirado JL (1996) Chem Mater 8:1429
6. Zhecheva E, Stoyanova R, Gorova M, Alcantara R, Morales J, Tirado JL (1997) Ionics 3:1
7. Kim DS, Lee CK, Kim H (2010) Solid State Sci 12:45
8. Kim KH, Kim KB (2008) Ultrason Sonochem 15:1019
9. Larcher D, Delobel B, Dantras-Laffont L, Simon E, Blach JF, Baudrin E (2010) Inorg Chem 49:10949
10. Yoshimura M, Suchanek W (1997) Solid State Ion 98:197
11. Larcher D, Palacín MR, Amatucci GG, Tarascon JM (1997) J Electrochem Soc 144:408
12. Khanderi J, Schneider JJ (2010) Eur J Inorg Chem 29:4591
13. Johnston WD, Heikes RR, Sestrich D (1958) J Phys Chem Solids 7:1
14. Orman HJ, Wiseman PJ (1986) Acta Crystallogr C 40:12
15. Delmas C, Fouassier C, Hagenmuller P (1980) Phys B 99:81
16. Gummow RJ, Liles DC, Thackeray MM, David WIF (1993) Mater Res Bull 28:1177
17. Morales J, Stoyanova R, Tirado JL, Zhecheva E (1994) J Solid State Chem 113:182
18. Shao-Horn Y, Hackney SA, Kahaian AJ, Thackeray MM (2002) J Solid State Chem 168:60
19. Jeong WT, Lee KS (2001) J Alloys Comp 322:205
20. Kosova NV, Anufrienko VF, Larina TV, Rougier A, Aymard L, Tarascon JM (2002) J Solid State Chem 165:56
21. Ninga LJ, Wua YP, Fanga SB, Rahm E, Holze R (2004) J Power Sources 133:229
22. Delmas C, Braconnier JJ, Hagenmuller P (1982) Mater Res Bull 17:117
23. Carlier D, Saadoune I, Croguennec L, Menetrier M, Suard E, Delmas C (2001) Solid State Ion 144:263
24. Paulsen JM, Dahn JR (1999) Solid State Ion 126:3
25. Komaba S, Yabuuchi N, Kawamoto Y (2009) Chem Lett 38: 954
26. Berthelot R, Carlier D, Pollet M, Doumerc JP, Delmas C (2009) Electrochem Solid-State Lett 12:A207
27. Kawamura T, Makidera M, Okada S, Koga K, Miura N, Yamaki J (2005) J Power Sources 146:27
28. Okubo M, Hosono E, Kudo T, Zhou HS, Honma I (2009) Solid State Ion 180:612
29. Zhecheva E, Stoyanova R (1994) J Solid State Chem 109:47
30. Zhecheva E, Stoyanova R (1991) Mater Res Bull. 26:1315
31. Kosova NV, Uvarov NF, Devyatkina ET, Avvakumov EG (2000) Solid State Ion 135:107
32. Delaplane RG, Ibers JA, Ferraro JR, Rush JJ (1969) J Chem Phys 50:1920
33. Rodrıguez-Carvajal J (1990) In: Satellite meeting on powder diffraction of the XV congress of the IUCr, p 127
34. Benedek R, Thackeray MM, van de Wall A (2008) Chem Mater 20:5485
35. Knop O, Reid KIG, Sutarno, Nakagawa Y (1968) Can. J. Chem 46:3463
36. Fernandez-Rodrigues JM, Hernan L, Morales J, Tirado JL (1988) Mater Res Bull 23:899
37. Zhecheva E, Stoyanova R, Angelov S (1990) Mater Chem Phys 25:361
38. Antolini E (1997) Mater Res Bull 32:9

39. Shinova E, Mandzhukova Ts, Grigorova E, Hristov M, Stoyanova R, Nihtianova D, Zhecheva E (2011) Solid State Ion. doi: 10.1016/j.ssi.2011.01.018
40. Shlyakhtin OA, Choi SH, Yoon YS, Oh Y-J (2004) Electrochim Acta 50:511
41. Choi SH, Kim J, Yoon YS (2004) J Power Sources 135:286
42. Reimers JN, Dahn JR (1992) J Electrochem Soc 139:2091
43. Reimers JN, Dahn JR, von Sacken U (1993) J Electrochem Soc 140:2752
44. Alcántara R, Ortiz GF, Lavela P, Tirado JL, Jaegermann W, Thissen A (2005) J Electroanal Chem 584:147
45. Alcántara R, Ortiz GF, Tirado JL, Stoyanova R, Zhecheva E, Ivanova S (2009) J Power Sources 194:494
46. Ménétrier M, Carlier D, Blangero D, Delmas C (2008) Electrochem Solid State Lett 11:A179